Lawrence Berkeley National Laboratory

LBL Publications

Title

Targeted Writing and Deleting of Magnetic Skyrmions in Two-Terminal Nanowire Devices

Permalink

https://escholarship.org/uc/item/2j58q346

Journal

Nano Letters, 21(3)

ISSN

1530-6984

Authors

Je, Soong-Geun

Thian, Dickson

Chen, Xiaoye

et al.

Publication Date

2021-02-10

DOI

10.1021/acs.nanolett.0c03686

Peer reviewed

eScholarship.org Powered by the California Digital Library
University of California

Targeted Writing and Deleting of Magnetic Skyrmions in Two-Terminal Nanowire Devices

Soong-Geun Je,[†,‡,§] Dickson Thian,[∥] Xiaoye Chen,[∥,¶] Lisen Huang,[∥,¶] Dae-Han Jeong,[**] Weilun Chao,[†] Ki-Suk Lee,[**] Jung-Il Hong,[‡] Anjan Soumyanarayanan,[*,∥,¶,††] and Mi-Young Im[*,†,‡]

[†]*Center for X-ray Optics, Lawrence Berkeley National Laboratory, Berkeley, California 94720, USA.*

[‡]*Department of Emerging Materials Science, DGIST, Daegu 42988, Korea.*

[§]*Department of Physics, Chonnam National University, Gwangju 61186, Korea.*

[∥]*Institute of Materials Research and Engineering, Agency for Science, Technology and Research, 138634 Singapore.*

[¶]*Data Storage Institute, Agency for Science, Technology and Research, 138634 Singapore.*

[**]*School of Materials Science and Engineering, Ulsan National Institute of Science and Technology, Ulsan 44919, Korea.*

[††]*Department of Physics, National University of Singapore, 117551 Singapore.*

*e-mail: anjan@imre.a-star.edu.sg; mim@lbl.gov

Abstract

Controllable writing and deleting of nanoscale magnetic skyrmions are key requirements for their use as information carriers for next-generation memory and computing technologies. While several schemes have been proposed, they require complex fabrication techniques or precisely tailored electrical inputs, which limits their long-term scalability. Here we demonstrate an alternative approach for writing and deleting skyrmions using conventional electrical pulses within a simple, two-terminal wire geometry. X-ray microscopy experiments and micromagnetic simulations establish the observed skyrmion creation and annihilation as arising from Joule heating and Oersted field effects of the current pulses, respectively. The unique characteristics of these writing and deleting schemes, such as spatial and temporal selectivity, together with the simplicity of the 2-terminal device architecture, provide a flexible and scalable route to the viable applications of skyrmions.

Keywords: Magnetic skyrmion, skyrmion writing, skyrmion deleting, Joule heating, Oersted field, Two-terminal device

Magnetic skyrmions are spatially localized spin textures with a well-defined topology.[1,2] Their nanoscale size and ambient stability in metallic thin films,[3-6] as well as efficient coupling to electrical currents,[7,8] are desirable inherent attributes that have prompted much excitement.[9] Notably, numerous recent device proposals seek to harness the skyrmion motion within a wire geometry[10] to realize applications in memory, logic, and unconventional computing.[11-13] An indispensable requirement for such devices is a spatially and temporally controlled scheme to write and delete skyrmions through robust and scalable techniques.

There has been considerable progress in writing magnetic skyrmions. Theoretical studies suggested that skyrmions can be created by spin currents.[14-16,19] Recent device-level write efforts have mostly utilized spin-orbit torques (SOTs) in application-relevant materials.[9,17-19] To facilitate the SOT-writing, the schemes require additional components, for example, geometric constrictions,[7,20,21] and defects.[22,23] While effective, however, these additional requirements lead to fabrication complexities in some cases, limiting their scalability.

On the contrary, the electrical deletion of skyrmions has thus far been lacking, and has been recognized as a critical pending challenge toward functional skyrmionic devices.[22,23] While two recent schemes have been reported for deterministic deletion and creation of skyrmions,[21,23] they have additional prerequisites, such as in-plane bias field[23] or precisely positioned nanostructures.[21] In the other, completely different current paths are required for writing and deletion,[21] increasing the complexity of device operation. Therefore, the need for the hour is to realize simple schemes for electrical skyrmion writing and deletion that may be readily adapted to myriad syrmion applications in a controlled fashion.

Here we present a simple and facile approach for writing and deleting skyrmions wherein an identical conventional current pulse is used for both operations. Crucial to this achievement is the harnessing of two by-products of electrical currents: Joule heating and Oersted field. By exploiting contrasting spatial and temporal properties of these two effects, we can achieve targeted operation, e.g., by simply reversing the pulse polarity. The ubiquitous character of these current-induced effects across material systems, coupled with minimalist requirements, offers much-needed attributes of scalability and broad applicability.

This work was performed on multilayer stacks of $[Pt(3)/Co(0.9)/MgO(1.5)]_{15}$ (Figure 1a, hereafter Pt/Co/MgO), which were sputtered on X-ray transparent Si_3N_4 membranes, and fabricated into 2 μm wide wires (see Supporting Information). The asymmetric Pt/Co/MgO stack hosts a sizeable interfacial Dzyaloshinskii-Moriya interaction (DMI), which can stabilize Néel-textured skyrmions at room temperature (RT).[4,24] To observe sub-100 nm magnetic skyrmions in Pt/Co/MgO multilayers, we employed full field magnetic transmission soft x-ray microscopy (MTXM) at the Advanced Light Source (XM-1, BL6.1.2).[25] Out-of-plane (OP) geometry (Figure 1b) is employed to detect the OP magnetization through X-ray magnetic circular dichroism. The imaging results, acquired at RT with in situ OP magnetic field $\mu_0 H$, are complemented by micromagnetic simulations using magnetic parameters determined from magnetometry measurements (see Supporting Information).

We begin by examining the equilibrium magnetization $M(\mu_0 H)$ of the Pt/Co/MgO multilayer, and corresponding MTXM images obtained over a wide wire pad (Figure 1c). The sheared hysteresis is characteristic of a multi-domain configuration at remanence as confirmed by the labyrinthine zero field (ZF) MTXM image. As $\mu_0 H$ is swept down from positive saturation (orange branch in Figure 1c), stripe domains nucleate at ~70 mT, which propagate to form a labyrinthine state. Meanwhile, on the upsweep (green branch in Figure 1c), increasing $\mu_0 H$ beyond zero results in the labyrinthine state transforming to oppositely magnetized stripes, which eventually shrink to a sparse array of sub-100 nm skyrmions. For the subsequent electrical writing experiments, the used magnetic fields correspond to the shaded region of Figure 1c, wherein the initial MTXM images are uniformly magnetized. Slight discrepancies between device level imaging and film-level $M(\mu_0 H)$ results may be attributed to the difference in the numbers of nucleation sites between the patterned wire[26] and the film.[3]

ELECTRICAL WRITING OF MAGNETIC SKYRMIONS

For electrical writing experiments, we begin by saturating the sample at large positive field, and lower it to a base field $\mu_0 H_b$ ranging from 80 to 126 mT (Figure 1c, shaded grey region) wherein the sample retains uniform magnetization (Figure 1d: top). Under these conditions,

the injection of a single current pulse (width ~30 ns, amplitude ~6.8×10^{11} A/m^2) results in the nucleation of skyrmions in the wire device (Figure 1d: bottom). We observe that the number of nucleated skyrmions varies considerably with $\mu_0 H_b$ as seen across the MTXM images (Figure 1d: bottom). The skyrmion nucleation is quantified in Figure 2b by measuring the density of created skyrmions, n_c, with respect to $\mu_0 H_b$. Below $\mu_0 H_b$ ~100 mT, the current pulse nucleates a dense skyrmion array, with density n_c > 5 μm^{-2} (e.g.. left in Figure 1d). Above $\mu_0 H_b$ ~100 mT, n_c drops sharply with increasing $\mu_0 H_b$ (middle in Figure 1d), and reaches zero at ~120 mT. Notably, the modulation of the electrical nucleation of skyrmions by the external magnetic field is distinct from those reported in previous works.[7,21-23,27]

Lateral currents within an asymmetric stack (e.g., Pt/Co/MgO) may produce a large SOT.[14] Such SOT governs skyrmion motion and, in some recent works, induces skyrmion nucleation.[21-23] However, the SOT-driven writing mechanisms cannot explain our results for the following reasons. First, our device does not have any geometric constrictions, positioned defects, or in-plane magnetic fields required for the SOT writing of skyrmions.[21,22] Second, unlike the peculiar bipolar pulse waveform used to achieve the dynamic SOT nucleation,[23] we use a conventional single pulse with a rectangular profile. Crucially, as we will show in Figure 3, the same pulse can be used for deletion of skyrmions which clearly rules out vectorial mechanisms associated with SOT. On the other hand, a plausible explanation may be the Joule heating effect and associated thermodynamics, which were previously shown to drive transitions from stripe domains to skyrmions.[27] For our case, simulation and analytical modelling suggest that current pulses used may induce a temperature rise ΔT ~220 K.[28]

To investigate the plausibility of heat-induced skyrmion nucleation, we performed micromagnetic simulations (see Methods). Typically, such simulations account for temperature effects solely by introducing randomly fluctuating fields.[29] However the ΔT would additionally change the magnetic parameters. To consider this effect, we measured the saturation magnetization $M_s(T)$ over 300-650 K (Figure 2a), and estimated the micromagnetic parameters at elevated temperatures using scaling relations with magnetization:[30-32] exchange stiffness $A \propto M_s^{1.8}$, interfacial DMI $D \propto M_s^{1.8}$ and uniaxial anisotropy $K_U \propto M_s^{3.03}$. The micromagnetic simulations were then performed following the recipe depicted in Figure 2b (details in Supporting Information). In particular, SOT effects

were not included. The system is first initialized to a uniformly magnetized state at $\mu_0 H_b$ (Figure 2c: top), subjected to a heating phase with rescaled parameters, and then restored to RT conditions (Figure 2c: bottom).

Figure 2c shows the simulation results for representative values of ΔT (111, 165 K) and $\mu_0 H_b$ (90, 120 mT). For ΔT = 165 K (Figure 2c, right), skyrmions are nucleated by the heat pulse, and their number decreases as $\mu_0 H_b$ increases. In contrast, the smaller heat pulse ΔT = 111 K (Figure 2c, left) does not create any skyrmions regardless of $\mu_0 H_b$. Figure 2d shows in further detail the simulated n_c with ΔT (100-250 K) and $\mu_0 H_b$ (80-120 mT). We find that a threshold ΔT > 150 K is required to nucleate any skyrmions, corresponding to a scaled magnetization $M_s(300 + \Delta T) \sim 0.9 M_s(300\ \text{K})$. Above this threshold, the field dependence of n_c is qualitatively consistent with the experimental data (Figure 1e). Overall, this indicates that Joule heating induced by current pulses is a viable explanation of the observed nucleation of skyrmions and the dependence of n_c on $\mu_0 H_b$.

Micromagnetic simulations further help to elucidate several aspects of heat-induced skyrmion energetics. First, Figure 2e shows the energy difference, ΔE, between the final and initial (ambient) states with varying ΔT and $\mu_0 H_b$. Notably ΔE is negative for most cases, with negligible variation over ΔT of 165-228 K, i.e., the skyrmion formation reduces the total energy with respect to that of the uniform state. This indicates that skyrmion nucleation is thermodynamically favoured (explored further in Conclusions), except near saturation ($\mu_0 H_b$ = 120 mT) wherein skyrmions may be metastable. Next, we note a slight qualitative difference in the nucleation phenomenology with ΔT (details in Supporting Information). For intermediate ΔT (<220 K), skyrmions are formed during the heating phase. However, for higher ΔT (>220 K), i.e., $M_s(T) < 0.8 M_s(300\ \text{K})$, fluctuations during the heat phase result in random magnetization, and skyrmions are formed only when the heat is turned off. Finally, simulations allow for a sequential study of the two heat-induced effects: thermal fluctuations and rescaling of magnetic parameters. Crucially, we find that no skyrmions are nucleated at any $\mu_0 H_b$ or ΔT if magnetic parameters are not rescaled (see Supporting Information). Together, these simulation insights strongly point to the thermodynamic origin of the observed nucleation of skyrmions. Finally, while the simulation results in Figure 2 are grain-

free, potential effects of pinning sites on heating and skyrmion nucleation are discussed in Supporting Information.

ELECTRICAL DELETION OF MAGNETIC SKYRMIONS

Meanwhile, we find that a slight modification of the skyrmion nucleation recipe can be used to annihilate skyrmions, as schematically shown in Figure 3a along with representative MTXM images. Here, the initial state consists of skyrmions created using the writing recipe at $\mu_0 H$ = 94 mT (Figure 3a: left). The magnetic field is then changed to a specific base field $\mu_0 H_b$ (Figure 3a: centre). The second pulse (deleting) is then injected to the wire, and the numbers of skyrmions before (N_{bef}) and after (N_{aft}) the current pulse are counted. Here we emphasize that identical current pulses are used for writing and deletion. As shown in Figure 3a, the number of skyrmions is reduced by ~50% following the applied current pulse. Note that the skyrmion annihilation has distint spatial asymmetry: skyrmion annihilation is more prominently on the right side of the wire. We quantify the efficacy of deletion by the annihilation rate $R_a \left(= 1 - N_{aft}/N_{bef} \right)$. Figure 3b shows a plot of R_a as a function of $\mu_0 H_b$. For lower $\mu_0 H_b$ (< 100 mT), R_a maintains a nearly constant negative value, indicating that skyrmions are instead nucleated by the current pulse (see Figure 1e). Above ~100 mT, R_a increases rapidly, consistent with the annihilation of existing skyrmions, and reaches unity near saturation (~130 mT). The observation that the same current pulse drives nucleation at lower $\mu_0 H_b$ and annihilation at higher $\mu_0 H_b$ suggests the existence of a cross-point field $\mu_0 H_c$ (~ 107 mT), corresponding to a dynamic equilibrium between these two phenomena.

The striking spatial asymmetry of skyrmion deletion (Figure 3a: right), mainly affecting the right side of the wire, is suggestive of an Oersted field driven phenomenon. Notably, reversing the current polarity flips the spatial asymmetry of skyrmion annihilation (Supporting Information), further supporting the Oersted field effect. Figure 3c shows the Oersted field profile during the current pulse, calculated by superposing the fields generated by current segments through the wire cross-section (Supporting Information). The Oersted field is sizable (up to ±40 mT) compared to $\mu_0 H_b$ (80-130 mT), and introduces considerable spatial asymmetry in the skyrmion distribution by increasing (decreasing) the net

perpendicular field on the right (left) of the wire as shown in Figure 1e and Figure 3b. Near the cross-point field $\mu_0 H_c$ ~107 mT, both nucleation and annihilation are likely equally effective, resulting in the clear spatial segregation of nucleation and annihilation as observed in Figures 1d and 3a. Therefore, our scheme has distinctive merits when operating near $\mu_0 H_c$ as one can selectively switch between nucleation and annihilation at a given spatial location simply by reversing the current polarity.

To elucidate the annihilation process, micromagnetic simulations were performed following the recipe depicted in Figure 4a (details in Supporting Information). Notably, while a current generates an instantaneous Oersted field, generating appreciable ΔT (c.f. Figure 2) requires a few tens of nanoseconds.[33] Our simulation recipe accounts for this lag by using an Oersted field (profile shown in Figure 3c) for the entire 30 ns pulse duration, followed by the heating phase introduced after a 10 ns delay. Figure 4b shows simulation results at several base fields $\mu_0 H_b$ of 110-140 mT, while Figure 4c displays the resulting annihilation rate R_a with respect to the lateral position x (defined in Figure 4b). Consistent with experiments (Figure 3b), the simulated R_a with $\mu_0 H_b$ and the deletion is more prominent on the right side of the wire. Meanwhile, we note that identical current pulses used in the skyrmion writing experiments would produce similar Oersted fields. Therefore, we have verified that such an Oersted field does not affect the simulated nucleation results (see Supporting Information). The contrasting influence of the Oersted field in the two cases is likely due to differences in initial conditions and the base field magnitude.

Interestingly, the simulations allow us to analyse the annihilation process in stepwise fashion (c.f. Figure 4a) to disentangle the various effects at play. The crucial finding is that all annihilation events in Figure 4 occur within the first 10 ns, wherein ΔT is assumed to be nearly zero (Supporting Information). No additional annihilation is observed at elevated temperatures with or without the Oersted field. In conjunction with the negative ΔE in Figure 2e, this suggests that Oersted field and Joule heating effects have counteracting outcomes in (de)stabilizing skyrmions. Notably, while thermal fluctuations have also been suggested to induce annihilation of skyrmions,[34] for our case, Joule heating induces skyrmion nucleation and prevents annihilation through rescaling of magnetic parameters over a wide temperature range. Therefore, the time delay between the Oersted field and heating effects, introduced to

reflect experimental reality, is crucial to enabling skyrmion deletion. Overall, while the inclusion of a more realistic current profile and material granularity may enable better quantitative agreement with experiments, the simulation results shown here establish the key mechanistic insights needed to interpret the skyrmion creation and annihilation observed in our wire devices.

CONCLUSIONS

Figure 5a,b summarizes the energetics of skyrmion nucleation and annihilation via Joule heating and Oersted field effects. First, at lower base fields, the skyrmion state becomes favorable relative to the uniform state, but nucleation is prevented by an energy barrier (Figure 5a: left). Magnetic parameters at elevated temperatures resulting from Joule heating reduce this barrier, and, incidentally, further lower the skyrmion energy, thereby enabling skyrmion nucleation (Figure 5a: center, right). The number of skyrmions formed depends on the energy difference of the uniform and skyrmion states, which may be controlled by adjusting the base field. Meanwhile, at higher base fields, the uniform state is comparable in energy with the skyrmion (Figure 5b: left), and the energy barrier now prevents skyrmion annihilation. However, the addition of an Oersted field pulls up the skyrmion energy, i.e., further destabilizes skyrmions, resulting in their annihilation regions with increased effective field

In summary, we have described our observations of the writing and deleting of skyrmions by lateral currents applied to a two-terminal wire device. A lateral electric current induces two thermodynamic effects: Joule heating and magnetic field. Our work harnesses the distinct spatial and temporal characteristics of these effects to write and delete skyrmions with efficacies that may be tuned by the external bias field. On one hand, Joule heating drives the nucleation of skyrmions, inherently stable at lower fields, by modifying magnetic parameters at elevated temperatures. On the other hand, the Oersted field preceding Joule heating enables annihilation of skyrmions in regions of higher fields. Together, our experiments and simulations provide a detailed energetic picture of these mechanisms that are generalizable to other skyrmion-hosting materials.

OUTLOOK

Our writing and deleting schemes are uniquely promising from a scalability perspective, considering the simplicity of device design and electrical inputs needed to implement the schemes. Their immense practical value will inspire immediate efforts towards deterministic and field-free skyrmion manipulation in such devices.[21-23] First, while both Joule heating and Oersted field effects may coexist and counteract, one could ensure for either of these to dominate by varying the length and amplitude of the current pulse.[21] Next, the requisite of external fields could be realized by appropriate use of magnetostatic effects.[35-38] While these schemes could be used together in skyrmionic racetrack devices,[9,21] each scheme can also be utilized for independently manipulating skyrmions. For example, the spatially selective nature of Oersted field-induced annihilation could be used to realize fabrication-free logic operations.[11] Finally, Joule heating presents itself as a promising technique to emulate a skyrmion bath or reservoir, providing a timely experimental platform for recently proposed novel computing architectures.[12,13]

METHODS

Micromagnetic Simulations. Simulations were performed using mumax[3] software package.[29] The effective medium theory was used to examine an equivalent reduced stack while retaining interlayer interactions.[8] The magnetic parameters were as follows (effective medium parameters in parenthesis): $A = 2.4 \times 10^{-11}$ J/m (4.0×10^{-12} J/m), $M_S = 1.59 \times 10^{6}$ A/m (2.64×10^{5} A/m), $K_u = 1.63 \times 10^{6}$ J/m^3 (5.21×10^{4} J/m^3) and $D = 1.76 \times 10^{-3}$ J/m^2 (2.93×10^{-4} J/m^2). These parameters were determined using procedures in previous works,[3,5,8] and are in line with published results on similar stacks.[4]

Joule Heating. Experimental determination of ΔT of the wire is challenging due to the low thermal conductivity of the membrane (substrate) and the short duration of the current pulse (30 ns). Therefore, ΔT is estimated using analytical model[28] with an assumption all charge is flowing the Pt layers, and is found to be ~220 K. Correspondingly, micromagnetic simulations were performed at elevated temperatures (up to ~600 K) to emulate the effect of heating. The elevated temperatures were reflected in: (a) the fluctuating thermal field in

mumax[3], and (b) rescaling of magnetic parameters to reflect their values at the elevated temperatures.

REFERENCES

1. Nagaosa, N.; Tokura, Y. Topological Properties and Dynamics of Magnetic Skyrmions. *Nat. Nanotechnol.* **2013,** 8, 899–911.

2. Soumyanarayanan, A.; Reyren, N.; Fert, A.; Panagopoulos, C. Emergent Phenomena Induced by Spin–Orbit Coupling at Surfaces and Interfaces. *Nature* **2016,** 539, 509–517.

3. Soumyanarayanan, A.; Raju, M.; Gonzalez Oyarce, A. L.; Tan, A. K. C.; Im, M.-Y.; Petrovic, A. P.; Ho, P.; Khoo, K. H.; Tran, M.; Gan, C. K.; Ernult, F.; Panagopoulos, C. Tunable Room-Temperature Magnetic Skyrmions in Ir/Fe/Co/Pt Multilayers. *Nat. Mater.* **2017,** 16, 898–904.

4. Boulle, O.; Vogel, J.; Yang, H.; Pizzini, S.; De Souza Chaves, D.; Locatelli, A.; Menteş, T. O.; Sala, A.; Buda-Prejbeanu, L. D.; Klein, O.; Belmeguenai, M.; Roussigné, Y.; Stashkevich, A.; Chérif, S. M.; Aballe, L.; Foerster, M.; Chshiev, M.; Auffret, S.; Miron, I. M.; Gaudin, G. Room-Temperature Chiral Magnetic Skyrmions in Ultrathin Magnetic Nanostructures. *Nat. Nanotechnol.* **2016,** 11, 449–454.

5. Moreau-Luchaire, C.; Moutafis, C.; Reyren, N.; Sampaio, J.; Vaz, C. A. F.; Van Horne, N.; Bouzehouane, K.; Garcia, K.; Deranlot, C.; Warnicke, P.; Wohlhüter, P.; George, J.-M.; Weigand, M.; Raabe, J.; Cros, V.; Fert, A. Additive Interfacial Chiral Interaction in Multilayers for Stabilization of Small Individual Skyrmions at Room Temperature. *Nat. Nanotechnol.* **2016,** 11, 444–448.

6. Je, S.-G.; Han, H.-S.; Kim, S. K.; Montoya, S. A.; Chao, W.; Hong, I.-S.; Fullerton, E. E.; Lee, K.-S.; Lee, K.-J.; Im, M.-Y.; Hong, J.-I. Direct Demonstration of Topological Stability of Magnetic Skyrmions *via* Topology Manipulation. *ACS Nano* **2020,** 14, 3251-3258.

7. Jiang, W. J.; Upadhyaya, P.; Zhang, W.; Yu, G. Q.; Jungfleisch, M. B.; Fradin, F. Y.; Pearson, J. E.; Tserkovnyak, Y.; Wang, K. L.; Heinonen, O.; te Velthuis, S. G. E.; Hoffmann, A. Blowing Magnetic Skyrmion Bubbles. *Science* **2015,** 349, 283–286.

8. Woo, S.; Litzius, K.; Krüger, B.; Im, M.-Y.; Caretta, L.; Richter, K.; Mann, M.;

Krone, A.; Reeve, R. M.; Weigand, M.; Agrawal, P.; Lemesh, I.; Mawass, M.-A.; Fischer, P.; Kläui, M.; Beach, G. S. D. Observation of Room-Temperature Magnetic Skyrmions and Their Current-Driven Dynamics in Ultrathin Metallic Ferromagnets. *Nat. Mater.* **2016,** 15, 501–506.

9. Fert, A., Reyren, N.; Cros, V. Magnetic Skyrmions: Advances in Physics and Potential Applications. *Nat. Rev. Mater.* **2017,** 2, 17031.

10. Parkin, S. S. P.; Hayasi, M.; Thomas, L. Magnetic Domain-Wall Racetrack Memory. *Science* **2008,** 320, 190-194.

11. Kang, W.; Huang, Y.; Zhang, X.; Zhou, Y.; Zhao, W. Skyrmion-Electronics: an Overview and Outlook. *Proc. IEEE* **2016,** 104, 2040–2061.

12. Pinna, D.; Abreu Araujo, F.; Kim, J.-V.; Cros, V.; Querlioz, D.; Bessiere, P.; Droulez, J.; Grollier, J. Skyrmion Gas Manipulation for Probabilistic Computing. *Phys. Rev. Appl.* **2018,** 9, 064018.

13. Prychynenko, D.; Sitte, M.; Litzius, K.; Krüger, B.; Bourianoff, G.; Kläui, M.; Sinova, J.; Everschor-Sitte, K. Magnetic Skyrmion as a Nonlinear Resistive Element: a Potential Building Block for Reservoir Computing. *Phys. Rev. Appl.* **2018,** 9, 014034.

14. Iwasaki, J.; Mochizuki, M.; Nagaosa, N. Current-Induced Skyrmion Dynamics in Constricted Geometries. *Nat. Nanotechnol.* **2013,** 8, 742-747.

15. Lin, S.-Z.; Reichhardt, C.; Saxena, A. Manipulation of Skyrmions in Nanodisks with a Current Pulse and Skyrmion Rectifier. *Appl. Phys. Lett.* **2013,** 102, 222405.

16. Lin, S.-Z.; Reichhardt, C.; Batista, C. D.; Saxena, A. Driven Skyrmions and Dynamical Transitions in Chiral Magnets. *Phys. Rev. Lett.* **2013,** 110, 207202.

17. Miron, I. M.; Garello, K.; Gaudin, G.; Zermatten, P. J.; Costache, M. V.; Auffret, S.; Bandiera, S.; Rodmacq, B.; Schuhl, A.; Gambardella, P. Perpendicular Switching of a Single Ferromagnetic Layer Induced by In-Plane Current Injection. *Nature* **2011,** 476, 189–193.

18. Iwasaki, J.; Mochizuki, M.; Nagaosa, N. Universal Current-Velocity Relation of

Skyrmion Motion in Chiral Magnets. *Nat. Commun.* **2013,** 4, 1463.

19. Sampaio, J.; Cros, V.; Rohart, S.; Thiaville, A.; Fert, A. Nucleation, Stability and Current-Induced Motion of Isolated Magnetic Skyrmions in Nanostructures. *Nat. Nanotechnol.* **2013,** 8, 839–844.

20. Hrabec, A.; Sampaio, J.; Belmeguenai, M.; Gross, I.; Weil, R.; Chérif, S. M.; Stashkevich, A.; Jacques, V.; Thiaville, A.; Rohart, S. Current-Induced Skyrmion Generation and Dynamics in Symmetric Bilayers. *Nat. Commun.* **2017,** 8, 15765.

21. Finizio, S; Zeissler, K.; Wintz, S.; Mayr, S.; Weßels, T.; Huxtable, A. J.; Burnell, G.; Marrows, C. H.; Raabe, J. Deterministic Field-Free Skyrmion Nucleation at a Nanoengineered Injector Device. *Nano Lett.* **2019,** 19, 7246–7255.

22. Büttner, F.; Lemesh, I.; Schneider, M.; Pfau, B.; Günther, C.; Hessing, P.; Geilhufe, J.; Caretta, L.; Engel, D.; Krüger, B.; Viefhaus, J.; Eisebitt, S.; Beach, G. S. D. Field-Free Deterministic Ultrafast Creation of Magnetic Skyrmions by Spin–Orbit Torques. *Nat. Nanotechnol.* **2017,** 12, 1040–1044.

23. Woo, S.; Song, K. M.; Zhang, X.; Ezawa, M.; Zhou, Y.; Liu, X.; Weigand, M.; Finizio, S.; Raabe, J.; Park, M.-C.; Lee, K.-Y.; Choi, J. W.; Min, B.-C.; Koo, H. C.; Chang, J. Deterministic Creation and Deletion of a Single Magnetic Skyrmion Observed by Direct Time-Resolved X-ray Microscopy. *Nat. Electron.* **2018,** 1, 288–296.

24. Juge, R.; Je, S.-G.; de Souza Chaves, D.; Buda-Prejbeanu, L. D.; Peña-Garcia, J.; Nath, J.; Miron, I. M.; Rana, K. G.; Aballe, L.; Foerster, M.; Genuzio, F.; Menteş, T. O.; Locatelli, A.; Maccherozzi, F.; Dhesi, S. S.; Belmeguenai, M.; Roussigné, Y.; Auffret, S.; Pizzini, S.; Gaudin, G.; Vogel, J.; Boulle, O. Current-Driven Skyrmion Dynamics and Drive-Dependent Skyrmion Hall Effect in an Ultrathin Film. *Phys. Rev. Appl.* **2019,** 12, 044007.

25. Chao, W.; Hartneck, B. D.; Liddle, J. A.; Anderson, E. H.; Attwood, D. T. Soft X-Ray Microscopy at a Spatial Resolution Better Than 15nm. *Nature* **2005,** 435, 1210–1213.

26. Woo, S.; Song, K. M.; Han, H.-S.; Jung, M.-S.; Im, M.-Y.; Lee, K.-S.; Song, K. S.;

Fischer, P.; Hong, J.-I.; Choi, J. W.; Min, B.-C.; Koo, H. C.; Chang, J. Spin-Orbit Torque-Driven Skyrmion Dynamics Revealed by Time-Resolved X-Ray Microscopy. *Nat. Commun.* **2017,** 8, 15573.

27. Lemesh, I.; Litzius, K.; Böttcher, M.; Bassirian, P.; Kerber, N.; Heinze, D.; Zázvorka, J.; Büttner, F.; Caretta, L.; Mann, M.; Weigand, M.; Finizio, S.; Raabe, S.; Im, M.-Y.; Stoll, H.; Schütz, G.; Dupé, B.; Kläui, M.; Beach, G. S. D. Current-Induced Skyrmion Generation through Morphological Thermal Transitions in Chiral Ferromagnetic Heterostructures. *Adv. Mater.* **2018,** 30, 1805461.

28. Fangohr, H.; Chernyshenko, D. S.; Franchin, M.; Fischbacher, T.; Meier, G. Joule Heating in Nanowires. *Phys. Rev. B* **2011**, 84, 054437.

29. Vansteenkiste, A.; Leliaert, J.; Dvornik, M.; Helsen, M.; Garcia-Sanchez, F.; Van Waeyenberge, B. The Design and Verification of MuMax3. *AIP Adv.* **2014,** 4, 107133.

30. Nembach, H. T.; Shaw, J. M.; Weiler, M.; Jué, E.; Silva, T. J. Linear Relation between Heisenberg Exchange and Interfacial Dzyaloshinskii–Moriya Interaction in Metal Films. *Nat. Phys.* **2015,** 11, 825-829.

31. Moreno, R.; Evans, R. F. L.; Khmelevskyi, S.; Muñoz, M. C.; Chantrell, R. W.; Chubykalo-Fesenko, O. Temperature-Dependent Exchange Stiffness and Domain Wall Width in Co. *Physical Review B* **2016,** 94, 104433.

32. Tomasello, R.; Guslienko, K. Y.; Ricci, M.; Giordano, A.; Barker, J.; Carpentieri, M.; Chubykalo-Fesenko, O.; Finocchio, G. Origin of Temperature and Field Dependence of Magnetic Skyrmion Size in Ultrathin Nanodots. *Physical Review B* **2018,** 97, 060402.

33. Kim, K.-J.; Lee, J.-C.; Choe, S.-B.; Shin, K.-H. Joule Heating in Ferromagnetic Nanowires: Prediction and Observation. *Appl. Phys. Lett.* **2008,** 92, 192509.

34. Legrand, W.; Maccariello, D.; Reyren, N.; Garcia, K.; Moutafis, C.; Moreau-Luchaire, C.; Collin, S.; Bouzehouane, K.; Cros, V.; Fert, A. Room-Temperature Current-Induced Generation and Motion of Sub100 nm Skyrmions. *Nano Lett.* **2017,** 17, 2703−2712.

35. Zeissler, K.; Mruczkiewicz, M.; Finizio, S.; Raabe, J.; Shepley, P. M.; Sadovnikov, A. V.; Nikitov, S. A.; Fallon, K.; McFadzean, S.; McVitie, S.; Moore, T. A.; Burnell, G.; Marrows, C. H. Pinning and Hysteresis in the Field Dependent Diameter Evolution of Skyrmions in Pt/Co/Ir Superlattice Stacks. *Sci. Rep.* **2017,** 7, 15125.

36. Juge, R.; Je, S.-G.; de Souza Chaves, D.; Pizzini, S.; Buda-Prejbeanu, L. D.; Aballe, L.; Foerster, M.; Locatelli, A.; Menteş, T. O.; Sala, A.; Maccherozzi, F.; Dhesi, S. S.; Auffret, S.; Gautier, A.; Gaudin, G.; Vogel, J.; Boulle, O. Magnetic Skyrmions in Confined Geometries: Effect of the Magnetic Field and the Disorder. *J. Magn. Magn. Mater.* **2018,** 455, 3–8.

37. Ho, P.; Tan, A. K.; Goolaup, S.; Oyarce, A. G.; Raju, M.; Huang, L.; Soumyanarayanan, A.; Panagopoulos, C. Geometrically Tailored Skyrmions at Zero Magnetic Field in Multilayered Nanostructures. *Phys. Rev. Appl.* **2019,** 11, 024064.

38. Finocchio, G.; Büttner, F.; Tomasello, R.; Carpentieri, M.; Kläui, M. Magnetic Skyrmions: from Fundamental to Applications. *J. Phys. D: Appl. Phys.* **2016,** 49, 423001.

ASSOCIATED CONTENT

Supporting Information

The supporting Information is available free of charge on the ACS Publication website at DOI:

Details of the experimental setup and micromagnetic simulation recipes for the skyrmion nucleation and annihilation (PDF)

AUTHOR INFORMATION

Corresponding Authors

*(M.-Y.I.) E-mail: mim@lbl.gov

*(A.S.) E-mail: anjan@imre.a-star.edu.sg

Notes

The authors declare no competing financial interest.

ACKNOWLEDGEMENTS

Works at the ALS were supported by U.S. Department of Energy (DE-AC02-05CH11231). S.-G.J. was supported by the National Research Foundation of Korea (NRF, Korea) grant funded by the Korea government (MSIT) (2020R1C1C1006194). M.-Y.I. acknowledges support by Lawrence Berkeley National Laboratory through the Laboratory Directed Research and Development (LDRD) Program. This work in Singapore was supported by the SpOT-LITE programme (Grant Nos. A1818g0042, A18A6b0057), funded by Singapore's RIE2020 initiatives, and by the Pharos skyrmion programme (Grant No. 1527400026) funded by A*STAR, Singapore. We also acknowledge the support of the National Supercomputing Centre (NSCC), Singapore for computational resources. K.-S.L. and D.-H.J. were supported by NRF of Korea grant funded MSIT (NRF-2019R1A2C2002996, NRF-

2016M3D1A1027831, and NRF-2019K1A3A7A09033400). J.-I.H. was supported by NRF of Korea grant funded MSIT (2020R1A2C2005932).

Figure 1

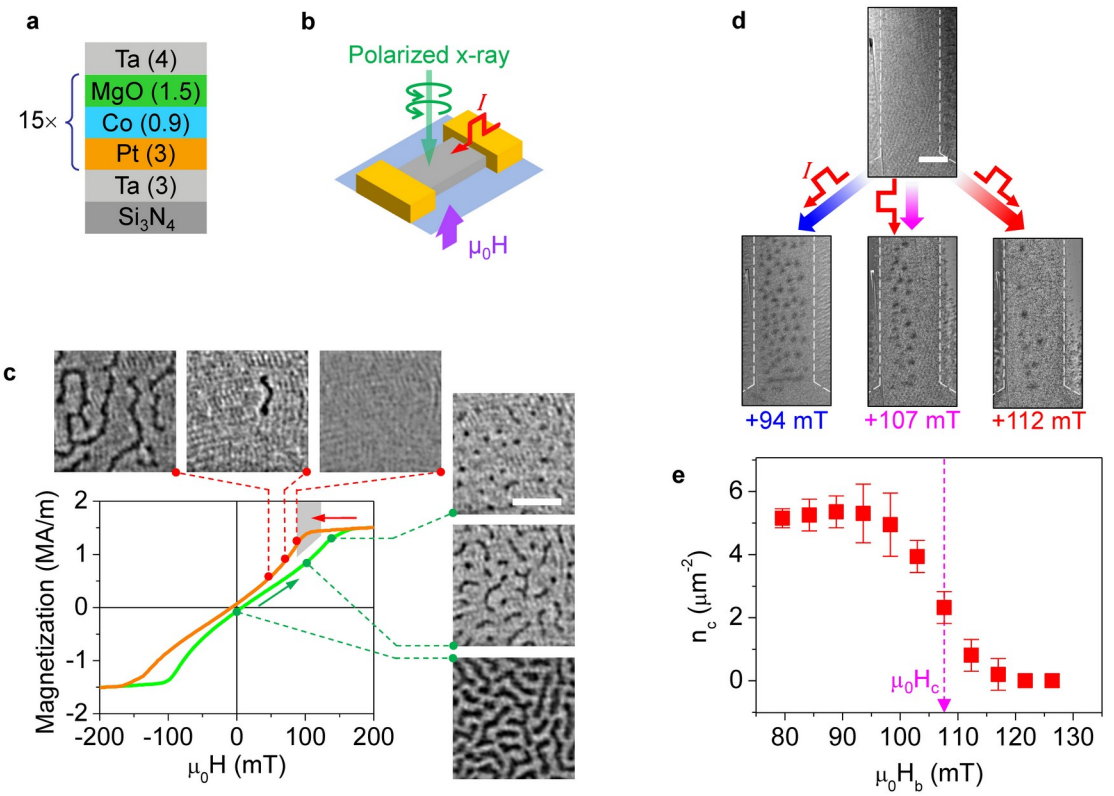

Figure 1: Experimental setup and current-driven skyrmion writing experiments. a, Schematic of the multilayer thin film used in this work (layer thickness in nm in parentheses). **b**, Schematic of the MTXM experimental setup. **c**, Hysteresis loop for OP magnetization, $M(\mu_0 H)$, with corresponding MTXM images (scale bar: 1 μm) at OP fields indicated by vertical dashed lines. Top three images (right to left) show the formation of chiral magnetic textures as $\mu_0 H$ is reduced from positive saturation ($+\mu_0 H_s$), while the bottom three (bottom to top) show their shrinking and disappearance as $\mu_0 H$ is increased from zero to $+\mu_0 H_s$. The shaded grey field region, corresponding to a uniformly magnetized state, indicates the base field range for experiments in Figure 2 and Figure 5. **d**, Typical examples of MTXM images (scale bar: 1 μm) of the wire before and after the current pulse. Top image shows the uniformly magnetized initial state at $\mu_0 H_b$. Bottom images show the final states (i.e., after a current pulse) at each $\mu_0 H_b$. Regarding the skyrmion size with respect to the external field, please see Supporting Information. **e**, Plot of the density, n_c, of skyrmions nucleated as per (d) against the base field $\mu_0 H_b$. The inferred crossover field (see Figure 3 and associated text) is labelled as $\mu_0 H_c$.

Figure 2

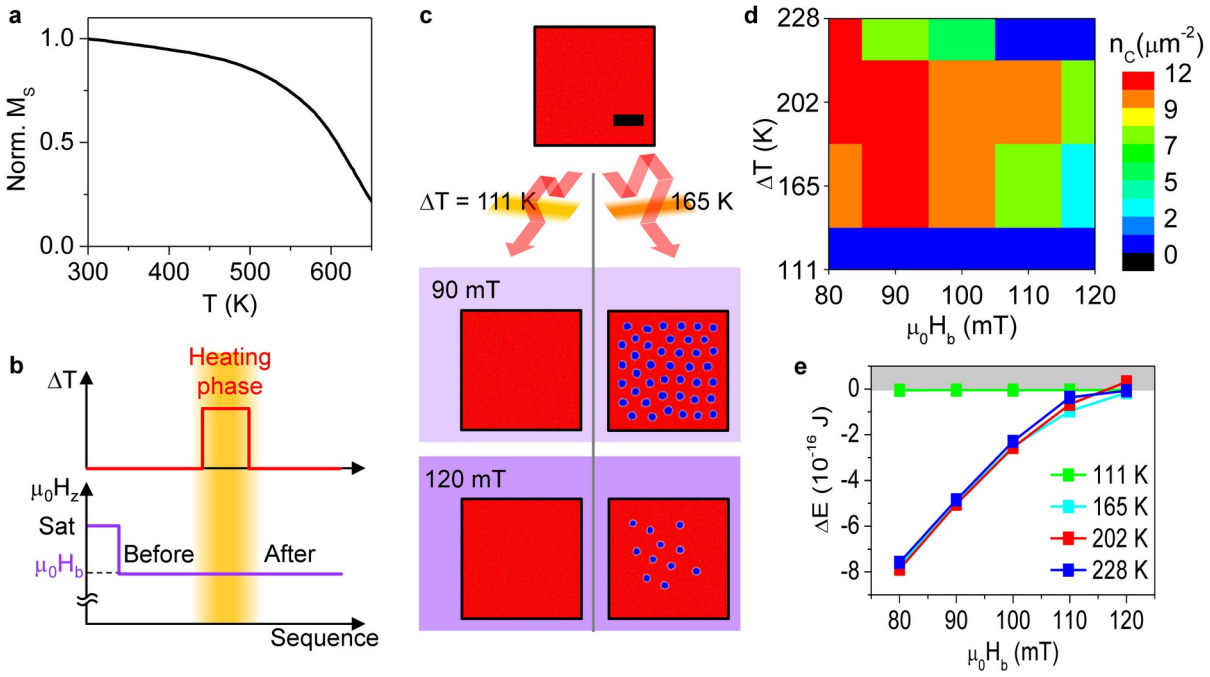

Figure 2: Simulations of heat-induced skyrmion nucleation. **a**, Measured variation of saturation magnetization (M_s) with temperature after normalizing to its 300 K value. This data is used along with scaling relations of magnetic parameters as inputs for Joule heating simulations. **b**, Schematic recipe used for micromagnetic simulations of Joule heating effects. **c**, Typical examples of simulation results for ΔT = 111 K, 165 K and $\mu_0 H_b$ = 90 mT, 120 mT, respectively (scale bar: 0.5 μm). Simulations are initialized at $\mu_0 H > \mu_0 H_s$, and the uniform state is brought to $\mu_0 H_b$ (c, top). During the heating phase (b, centre), the simulated temperature is raised by ΔT and magnetic parameters are rescaled (see text, Figure 4a). Skyrmions are nucleated in some cases (c, right), and persist when RT conditions are restored. **d**, Color plot showing the nucleated skyrmion density, n_c, as a function of ΔT and $\mu_0 H_b$ (the latter c.f. Figure 1e). **e**, Micromagnetic energy difference, ΔE, between final (skyrmion nucleated) and initial (uniform) states for various ΔT and $\mu_0 H_b$. The final state is more stable if ΔE < 0 (note: ΔE = 0 for ΔT = 111 K as the initial and final states are identical).

Figure 3

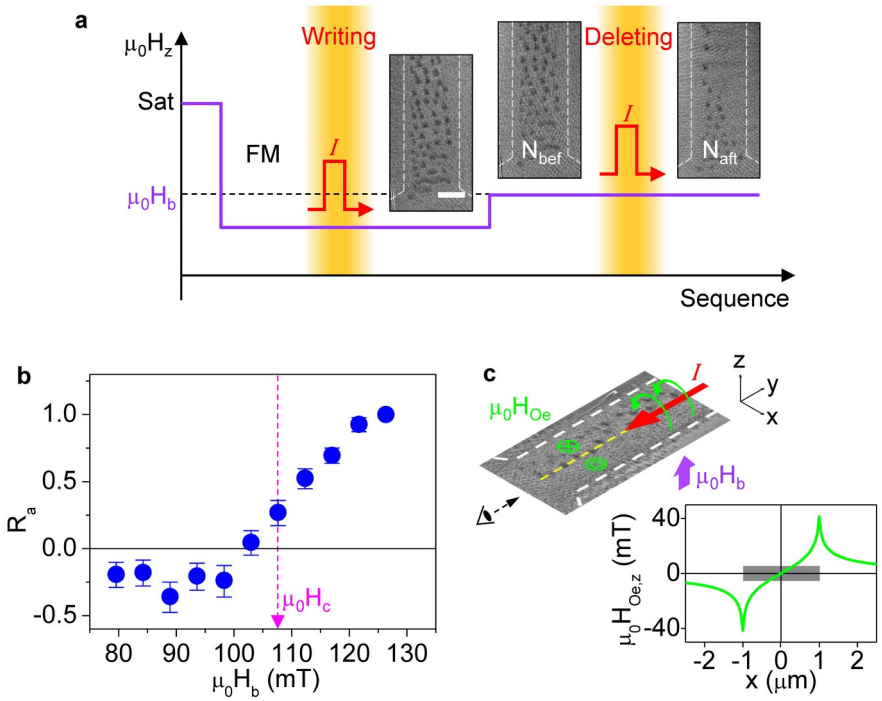

Figure 3: Current-driven skyrmion deletion experiments. a, Recipe used for skyrmion deletion, with representative MTXM images (scale bar: 1 μm) as insets. **b**, Plot of the skyrmion annihilation rate, $R_a \equiv 1 - N_{aft}/N_{bef}$, with varying base field $\mu_0 H_b$. The inferred crossover field, $\mu_0 H_c$, is indicated (c.f. Figure 1e, see figure caption). **c**, Plot of the expected Oersted field profile (inset shows schematic) generated by a current applied along $-\hat{y}$ (red arrow) as a function of the transverse position x across the wire.

Figure 4

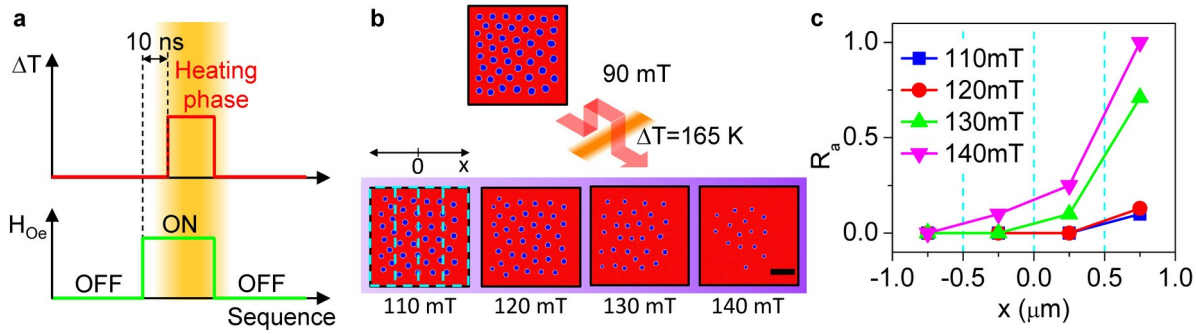

Figure 4: Simulations of Oersted field-induced skyrmion annihilation. a, Schematic recipe used for simulating Oersted field effect with Joule heating (details in Supporting Information). The current pulse is modelled as inducing an Oersted field (profile in Figure 3c) for the entire 30 ns duration (bottom) and Joule heating for the latter 20 ns (top). **b**, Simulated magnetization before (top) and after (bottom) the base field is raised to $\mu_0 H_b$ (110-140 mT), and the recipe in (a) is used. Skyrmions are annihilated in some cases (bottom right). **c**, Skyrmion annihilation rate R_a plotted as a function of transverse position, x, across the wire for several base fields $\mu_0 H_b$. R_a is determined by the number of skyrmions in the dashed boxes in Figure 4b. The four sections in Figure 4c divided by the cyan dashed lines correspond to the dashed boxes in Figure 4b.

Figure 5

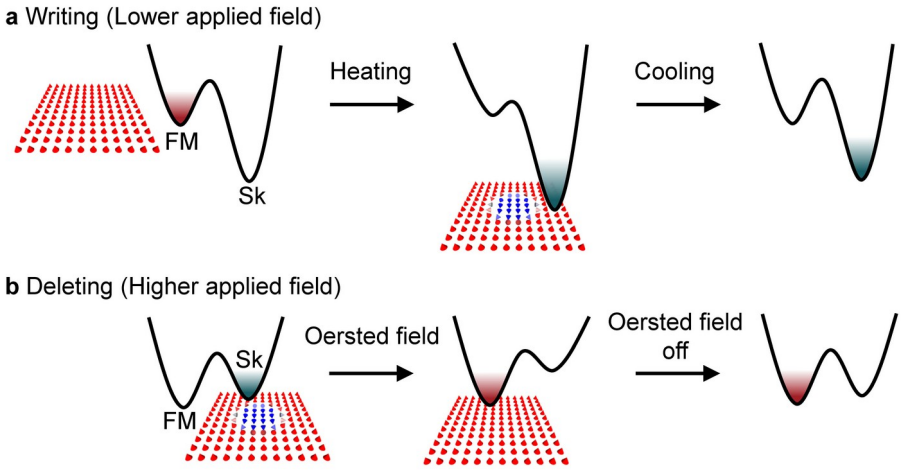

Figure 5: Schematic energetics for writing and deleting mechanism. a, Skyrmions are written onto the uniform state by injecting a current pulse at lower $\mu_0 H_b$, wherein they are energetically favored. Joule heating induced by the current pulse drives their nucleation by lowering the energy barrier. **b**, Deletion is effective at higher $\mu_0 H_b$ where the uniform and skyrmion states are comparable in energy. An Oersted field added into the base field raises the energy of the skyrmion state, and thereby triggers annihilation of the skyrmion by injecting a current pulse.